J. Fluid Mech. (1972), *vol.* 56, *part* 4, *pp.* 741–752
Printed in Great Britain

Heat transfer from hypersonic turbulent flow at a wedge compression corner

By G. T. COLEMAN AND J. L. STOLLERY
Department of Aeronautics, Imperial College, London

(Received 16 June 1972 and in revised form 27 September 1972)

A hypersonic gun tunnel has been used to measure the heat-transfer-rate distribution over a compression corner under turbulent boundary-layer conditions. Attached, incipient and separated flows are considered. The results are compared with other experimental data and with the predictions of a simple theory.

1. Introduction

Elfstrom (1972) has presented the results of a shock-boundary-layer study at a Mach number of 9 using a compression corner model to simulate a deflected control surface. He measured the pressure distributions for both attached and separated flows, paying particular attention to the incipient separation condition. His work confirms and extends the data of Batham (1972) and others in showing the extreme resistance of a hypersonic turbulent boundary layer to separation. Typically a wedge angle exceeding 30° is needed at $M = 9$ to cause separation. Below the separation angle the upstream influence of the corner is less than a single boundary-layer thickness. The heat-transfer results presented here confirm these observations and are complementary to Elfstrom's study. The distributions of heat-transfer rate and pressure, when non-dimensionalized by the appropriate flat-plate values, are very similar in form. This similarity even extends to the separated flow regions where, in contrast to laminar flow, the heat transfer increases. The rise in heat-transfer rate in the separated region has been noted by previous investigators, including Gadd, Cope & Attridge (1960), Holloway, Sterrett & Creekmore (1965) and Holden (1972). The data presented here give more detailed information on the heat-transfer rate in the separated region in addition to extending the Mach-number and Reynolds-number range covered in the previous tests.

2. Apparatus

The measurements were made at a Mach number of 9 in the Imperial College no. 2 Gun Tunnel using nitrogen as the test gas. The design, operation and performance of the tunnel has been described by Needham, Elfstrom & Stollery (1970). The free-stream test conditions are given in table 1, where the subscripts ∞, 0 and w refer to free-stream, reservoir and wall conditions respectively, Re_L is the Reynolds number based on L, the length of the flat plate to the hinge line, and the other symbols are standard.

M_∞	Re'_∞ (cm^{-1})	Re_L	T_0 (°K)	T_∞ (°K)	T_w (°K)
9·22	$0{\cdot}47 \times 10^6$	$26{\cdot}4 \times 10^6$	1070	64·5	295
8·96	$0{\cdot}12 \times 10^6$	$5{\cdot}9 \times 10^6$	1070	65·5	295

TABLE 1. Free-stream conditions for heat-transfer measurements

The model was a sharp flat plate with an adjustable trailing-edge flap; both were instrumented along the centre-line with closely spaced thin-film platinum-on-glass surface temperature gauges. The signals were converted to measure the heat-transfer rate by electrical analog circuits and the outputs recorded on oscilloscopes.

3. Theory

The very severe adverse pressure gradients of the present experiments provide a stringent test of any theory of compressible turbulent boundary layers. The momentum-integral technique, developed by Todisco & Reeves (1969) from the pioneering work of Lees & Reeves (1964) for laminar flow, seems capable of tackling this problem but further progress requires a detailed knowledge of velocity and temperature profile development in an adverse pressure gradient.

Theoretical prediction methods often begin with a known inviscid pressure distribution and finally use some form of Reynolds analogy to predict the heat-transfer rate. Roshko & Thomke (1969) and Ceresuela & Coulomb (1970), amongst others, have pointed out that much of the turbulent boundary layer behaves as an inviscid rotational stream. Elfstrom (1972) has used this idea in devising a simple method for predicting the pressure distribution with attached flow over the flap. A method of calculating the heat-transfer rate from the given initial conditions ahead of the hinge line and the predicted pressure distribution is now required.

Many investigators have noted that the behaviour of the turbulent boundary layer in strong pressure gradients at hypersonic speeds can be described in terms of local conditions. The flow around the nose of a blunt body is a classic example in which the main effect of the (favourable) pressure gradient is assumed to be on the thickness and not on the shape of the boundary-layer profiles. This encourages the use of 'local flat plate' solutions based on fluid properties at the edge of the boundary layer and the local thickness (δ). Although a method of this type must fail at and beyond incipient separation it may well be useful for attached flow.

The analysis followed here is similar to those originally proposed by Ambrok (1957) and Walker (1960) with later development by Back & Cuffel (1970). If the energy thickness ϕ is defined by

$$\phi = \int_0^\delta \frac{\rho u}{\rho_e u_e}\left(1 - \frac{H(y)}{He}\right) dy, \tag{1}$$

where H is the total enthalpy, the subscript e refers to conditions at the edge of

the boundary layer and the other symbols are standard, then the integral form of the energy equation (heat balance) may be written as

$$d(\rho_e u_e H_e \phi)/dx = \dot{q}, \tag{2}$$

where $\dot{q}$ is the heat-transfer rate to the surface and x the distance along the flat plate from the leading edge. To complete the solution a relation between $\dot{q}$ and ϕ is needed. Ambrok suggested the use of the flat-plate value for the Stanton number St_e based on local conditions, i.e.

$$St_e \sim \{(\rho_e u_e/\mu_e)\,\phi\}^{-\frac{1}{4}}, \tag{3}$$

which is analogous to the skin-friction equation in terms of the momentum-thickness Reynolds number. According to Back & Cuffel, equation (3) is a reasonable description of measurements subsequently made in both accelerating and decelerating flows.

To obtain the precise form of (3) we made use of the Reynolds analogy

$$\dot{q}/\rho_e u_e(h_r - h_w) = St_e = \tfrac{1}{2}C_f Pr^{-\frac{2}{3}}, \tag{4}$$

where h_r and h_w are the recovery and wall values of the static enthalpy h. The local skin-friction coefficient is given by

$$\tfrac{1}{2}C_f = 0{\cdot}013 Re_\theta^{-\frac{1}{4}} (\mu^*/\mu_e)^{\frac{1}{4}} \rho^*/\rho_e, \tag{5}$$

the values denoted by * being evaluated at Eckert's reference enthalpy condition. For flat-plate flow, the energy and momentum thicknesses are related by

$$\theta = \frac{H_e Pr^{\frac{2}{3}}}{h_r - h_w}\phi \tag{6}$$

provided that the Crocco relations holds. Equations (5) and (6) may be substituted in (3) with the further assumption that $\mu \sim T^{0{\cdot}76}$ to give

$$\frac{\dot{q} Pr^{\frac{2}{3}}}{\rho_e u_e(h_r - h_w)} = 0{\cdot}013\left(\frac{T^*}{T_e}\right)^{-0{\cdot}81}\left(\frac{h_r - h_w}{H_e Pr^{\frac{2}{3}}}\right)^{\frac{1}{4}} Re_\phi^{-\frac{1}{4}}. \tag{7}$$

Equation (7) can be re-written in the form

$$\dot{q} = f(x)/(\rho_e u_e H_e \phi)^{\frac{1}{4}}, \tag{8}$$

substituted in (2) and integrated to produce an expression for ϕ which may then be introduced into (8). The result, which was also obtained by Walker, is

$$\dot{q} = \frac{0{\cdot}0296}{Pr^{\frac{2}{3}}} \frac{\rho_e u_e \mu_e^{\frac{1}{4}}(h_r - h_w)^{\frac{5}{4}}(T^*/T_e)^{-0{\cdot}81}}{\left[\int_0^x \rho_e u_e \mu_e^{\frac{1}{4}}(h_r - h_w)^{\frac{5}{4}}(T^*/T_e)^{-0{\cdot}81}\,dx\right]^{\frac{1}{5}}}. \tag{9}$$

For isothermal wall conditions, as in the present tests, $h_r - h_w$ is a constant and may be cancelled. The variation of $\mu_e^{\frac{1}{20}}$ and $(T^*/T_e)^{-0{\cdot}16}$ in the denominator is usually insignificant, so that (9) may be simplified to

$$\frac{\dot{q}}{\rho_e u_e(h_r - h_w)} = St_e = \frac{0{\cdot}0296}{Pr^{\frac{2}{3}}}\left(\frac{T^*}{T_e}\right)^{-0{\cdot}65} Re_X^{-\frac{1}{5}}, \tag{10}$$

where $$Re_X = \rho_e u_e X/\mu_e \quad \text{with} \quad \rho_e u_e X = \int_0^X \rho_e u_e dx \tag{11}$$

and $$T^*/T_e = 0{\cdot}5\,(T_w/T_e + 1) + 0{\cdot}044 r M_e^2. \tag{12}$$

Of course, the lower bound of integration in the definition of X [equation (11)] must be the effective origin of the turbulent boundary layer.

Equation (10) may be expressed in terms of the heat transfer to a flat plate at zero incidence in a uniform free stream ($\dot{q}_{fp}$). If we take

$$\frac{\dot{q}_{fp}}{\rho_\infty u_\infty (h_r - h_w)} = \frac{0{\cdot}0296}{Pr^{\frac{2}{3}}} \left(\frac{T^*}{T_\infty}\right)^{-0{\cdot}65} \left\{\frac{\rho_\infty u_\infty x}{\mu_\infty}\right\}^{-\frac{1}{5}}, \tag{13}$$

then

$$\frac{\dot{q}}{\dot{q}_{fp}} = \frac{\rho_e u_e}{\rho_\infty u_\infty} \left[\frac{(1 + T_w/T_{0\infty}) + \frac{1}{5}M_\infty^2 (0{\cdot}4 + T_w/T_{0\infty})}{(1 + T_w/T_{0\infty}) + \frac{1}{5}M_e^2 (0{\cdot}4 + T_w/T_{0\infty})}\right]^{0{\cdot}65} \left\{\frac{\rho_\infty u_\infty x}{\int_0^X \rho_e u_e dx} \frac{\mu_e}{\mu_\infty}\right\}^{\frac{1}{5}}, \tag{14}$$

since $T_{0\infty} = T_{0e}$ for homenergic external flow and

$$\frac{T^*}{T} = 0{\cdot}5\left[\left(1 + \frac{T_w}{T_{0\infty}}\right) + \frac{M^2}{5}\left(0{\cdot}4 + \frac{T_w}{T_{0\infty}}\right)\right] \tag{12a}$$

assuming that the recovery factor $r = 0{\cdot}9$. For cold-wall hypersonic flow the relation (14) suggests that the increase in heat-transfer rate over compression surfaces is primarily due to the increased local density and reduced local Mach number. Similar comments may be made for expansion surfaces.

For the compression corner experiments reported here the chord of the flap was modest in comparison with the length of the flat plate ahead of the hinge line. Thus the last bracketed term in (14) is approximately unity. Moreover, the tests were run under cold-wall conditions ($T_w/T_{0\infty} \simeq 0{\cdot}3$), so that the dominant term in (12a) is the term in $\frac{1}{5}M^2$. Hence (14) may be reduced to a very approximate form, namely

$$\frac{\dot{q}}{\dot{q}_{fp}} \simeq \frac{\rho_e u_e}{\rho_\infty u_\infty} \left[\frac{M_\infty}{M_e}\right]^{1{\cdot}3}. \tag{15}$$

Using the oblique shock relations to express the various ratios in terms of the pressure ratio P equation (15) becomes

$$Q = \frac{\dot{q}}{\dot{q}_{fp}} \simeq \left(\frac{6P+1}{P+6}\right) \frac{[M_\infty^2 P(P+6)]^{0{\cdot}65}}{[(6P+1)M_\infty^2 - 5(P^2-1)]^{0{\cdot}15} [M_\infty^2 (6P+1)]^{0{\cdot}5}}. \tag{16}$$

For small P equation (16) suggests that $Q \simeq P$; however the turbulent boundary layer can withstand large pressure rises before separating. For $P \gg 1$ equation (16) may be simplified to

$$Q \simeq 6\tfrac{1}{2} P^{0{\cdot}65} [6 - 5P/M_\infty^2]^{-0{\cdot}15}, \tag{17}$$

which indicates that as P increases Q will follow the same pattern but have a smaller magnitude. It is interesting to note that Back & Cuffel suggested the relationship $Q \simeq P^{0{\cdot}85}$, which predicts values very similar to those calculated using (17).

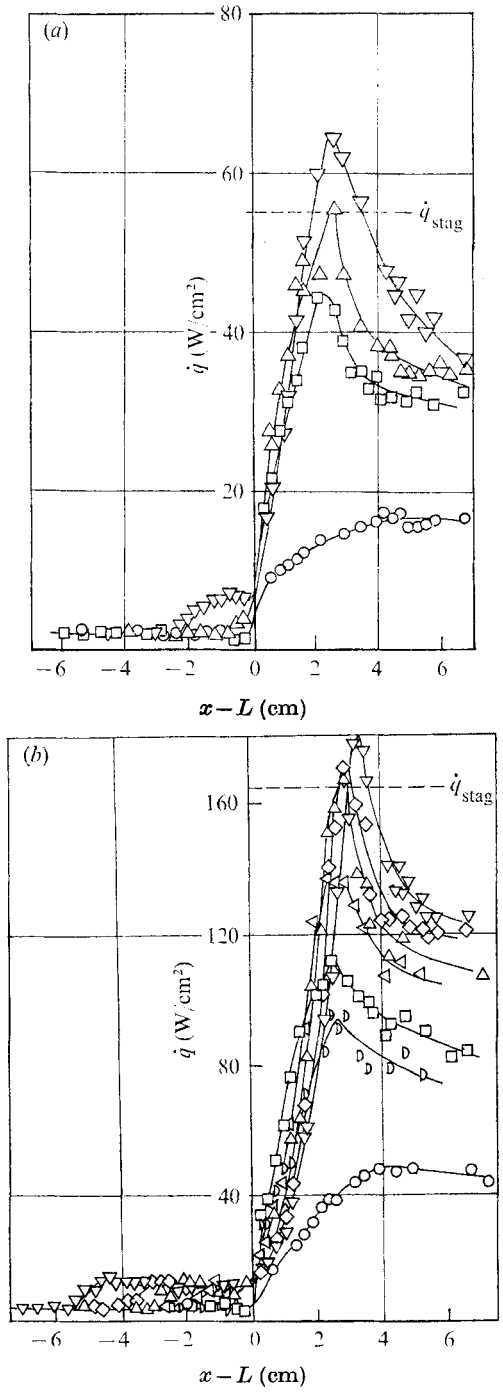

FIGURE 2. Heat-transfer-rate measurement at a wedge compression corner. (*a*) $M_\infty = 8{\cdot}96$, $Re_\infty = 1{\cdot}2 \times 10^5\ \text{cm}^{-1}$, $T_0 = 1070\ ^\circ\text{K}$, $T_w = 295\ ^\circ\text{K}$. (*b*) $M_\infty = 9{\cdot}22$, $Re_\infty = 4{\cdot}7 \times 10^5\ \text{cm}^{-1}$, $T_0 = 1070\ ^\circ\text{K}$, $T_w = 295\ ^\circ\text{K}$.

α	▽ 38°	◇ 36°	△ 34°	◁ 32°	□ 30°	◗ 26°	○ 15°

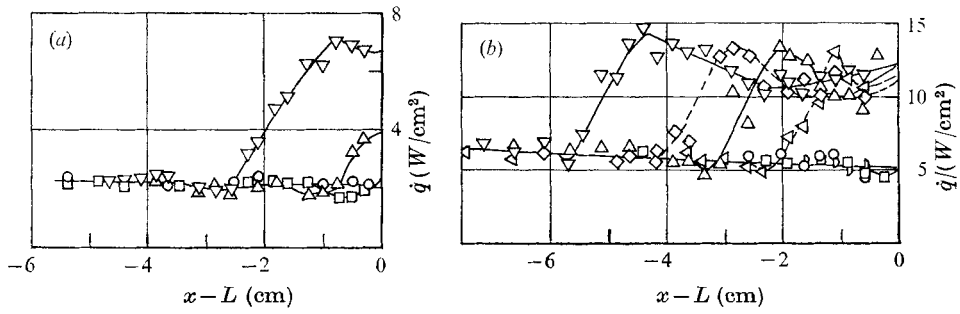

FIGURE 3. Heat-transfer-rate distributions ahead of the hinge line at a wedge compression corner. (*a*) $M_\infty = 8{\cdot}96$, $Re_\infty = 1{\cdot}2 \times 10^5\,\mathrm{cm}^{-1}$, $T_0 = 1070\,^\circ\mathrm{K}$, $T_w = 295\,^\circ\mathrm{K}$. (*b*) $M_\infty = 9{\cdot}22$, $Re_\infty = 4{\cdot}7 \times 10^5/\mathrm{cm}$, $T_0 = 1070\,^\circ\mathrm{K}$, $T_w = 295\,^\circ\mathrm{K}$. Symbols as in figure 2.

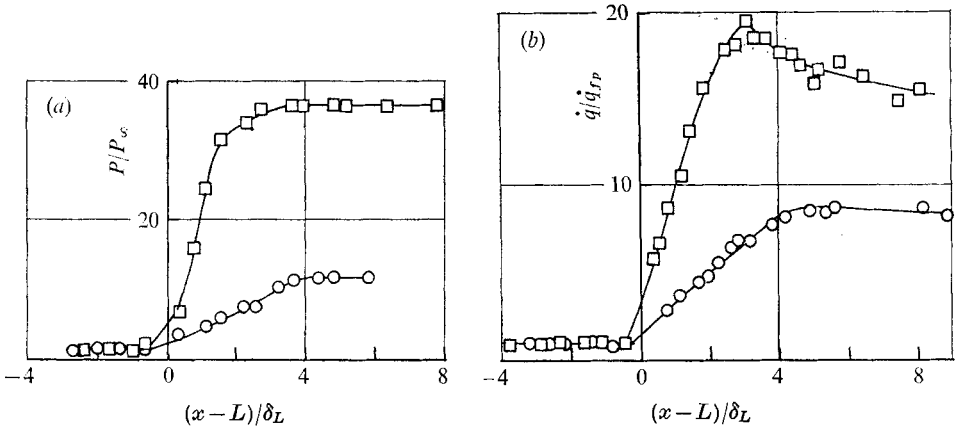

FIGURE 4. Comparison of pressure and heat-transfer distributions for attached flow at wedge compression corner. $M_\infty = 9{\cdot}22$, $Re_\infty = 4{\cdot}7 \times 10^5\,\mathrm{cm}^{-1}$, $T_0 = 1070\,^\circ\mathrm{K}$, $T_w = 295\,^\circ\mathrm{K}$. (*a*) Pressure distributions (Elfstrom). (*b*) Heat-transfer distributions (present study). □, $\alpha = 30°$; ○, $\alpha = 15°$.

4. Results and discussion

Typical schlieren pictures of the flow are shown in figure 1 (plate 1) for both attached and separated flow. The raw heat-transfer data, which have all been tabulated by Coleman & Stollery (1972), are plotted in figure 2 for two different Reynolds numbers. The figure shows that the heat-transfer rate just ahead of the hinge line increases as separation occurs. Using this increase as a criterion, the flow at flap angles up to and including $\alpha = 30°$ is attached and the incipient separation angle lies between 30° and 32°. The increase in heat-transfer rate in the separated region is of particular interest because it is in complete contrast to the laminar result. This effect was suggested by Chapman (1956) but with the reservation that it might not occur at high Mach numbers. Experimental evidence of the increase has since been found by Gadd *et al.* (1960) at a Mach number of 2·44, by Holloway *et al.* (1965) at a Mach number of 6, by Appels & Backx (1971) at $M = 11{\cdot}8$ and more recently by Holden (1972) at Mach numbers in the range

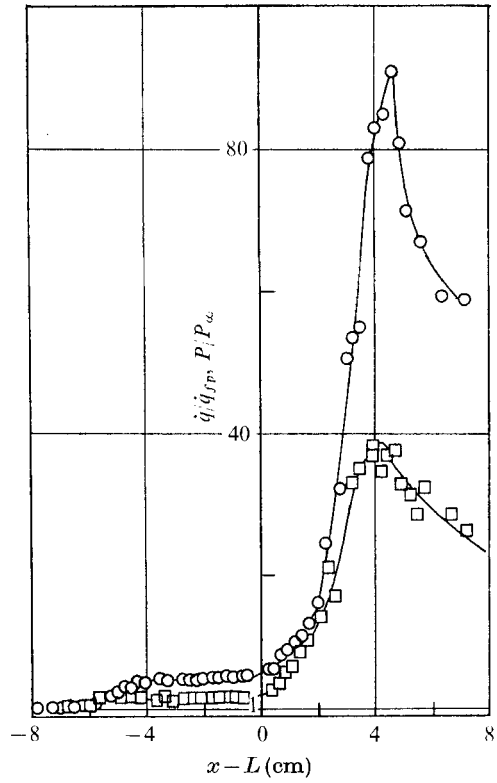

FIGURE 5. Comparison of pressure and heat-transfer distributions for separated flow at a wedge compression corner, under forced transition conditions. $M_\infty = 9{\cdot}22, Re_\infty = 4{\cdot}7 \times 10^5$ cm^{-1}, $T_0 = 1070$ °K, $T_w = 295$ °K, $\alpha = 38°$. ○, pressure data; □, heat-transfer data.

6·5–13·0. Details of the heat-transfer distribution in the separated region ahead of the hinge line are shown in figure 3.

An important feature of separated flow is the high peak heat-transfer rate just downstream of reattachment, with values exceeding the two-dimensional stagnation point ($\dot{q}_{\text{stag}}$) value for laminar flow. These peaks correspond to the large pressure overshoots measured by Elfstrom. For attached flow the similarity between the pressure and heat-transfer distributions is evident from figure 4. The upstream influence of the corner is extremely small right up to the incipient separation angle. To eliminate any differences of transition location between the pressure model of Elfstrom and the heat-transfer model of the present study, some tests were made with forced transition. The boundary layer was tripped by a row of vortex generators 1 cm from the leading edge. Figure 5 shows a comparison between the pressure and heat-transfer distributions for separated flow with forced transition. Near separation both distributions rise, reaching a plateau value in the fully separated region. A very rapid rise through reattachment to a peak is followed by a drop towards the trailing edge of the flap.

The effect of increasing the Reynolds number based on the boundary-layer thickness δ_L at the hinge line (figure 6) is to extend the separated region significantly once separation has occurred and to reduce the incipient separation

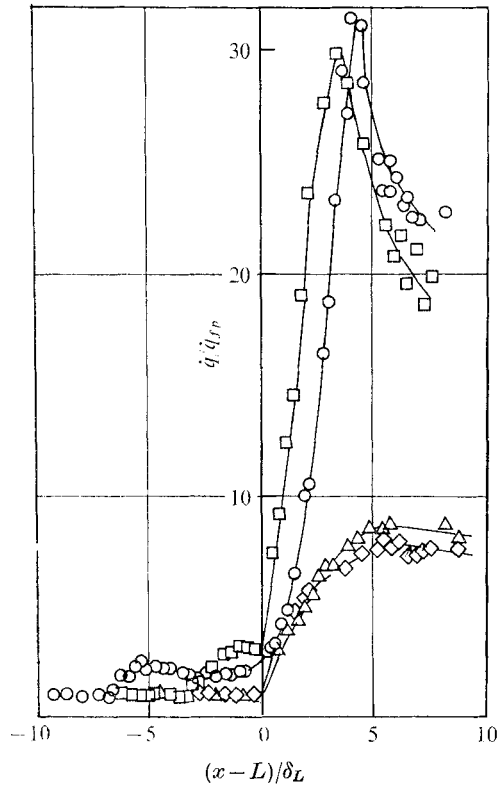

FIGURE 6. Effect of Reynolds number on heat-transfer-rate distributions at a wedge compression corner. $Re_{\delta_L} = 0{\cdot}93 \times 10^5$: □, $\alpha = 38°$ (separated); ◇, $\alpha = 15°$ (attached). $Re_{\delta_L} = 3{\cdot}8 \times 10^5$: ○, $\alpha = 38°$ (separated); △, $\alpha = 15°$ (attached).

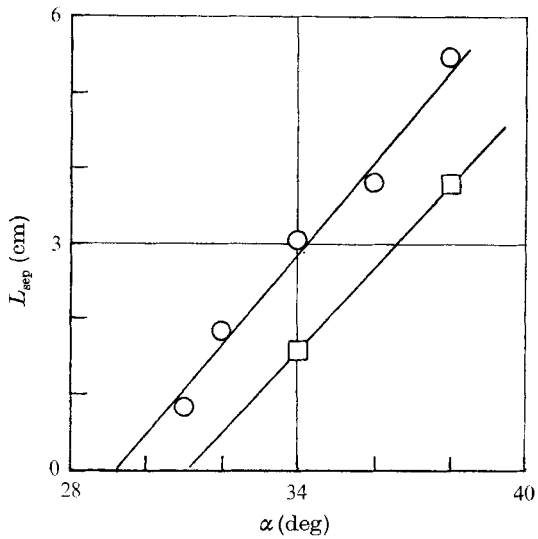

FIGURE 7. Determination of incipient separation angle by extrapolation of the separation length L_{sep} measured from schlieren pictures, to zero. ○, $Re_{\delta_L} = 3.8 \times 10^5$; □, $Re_{\delta_L} = 0{\cdot}93 \times 10^5$.

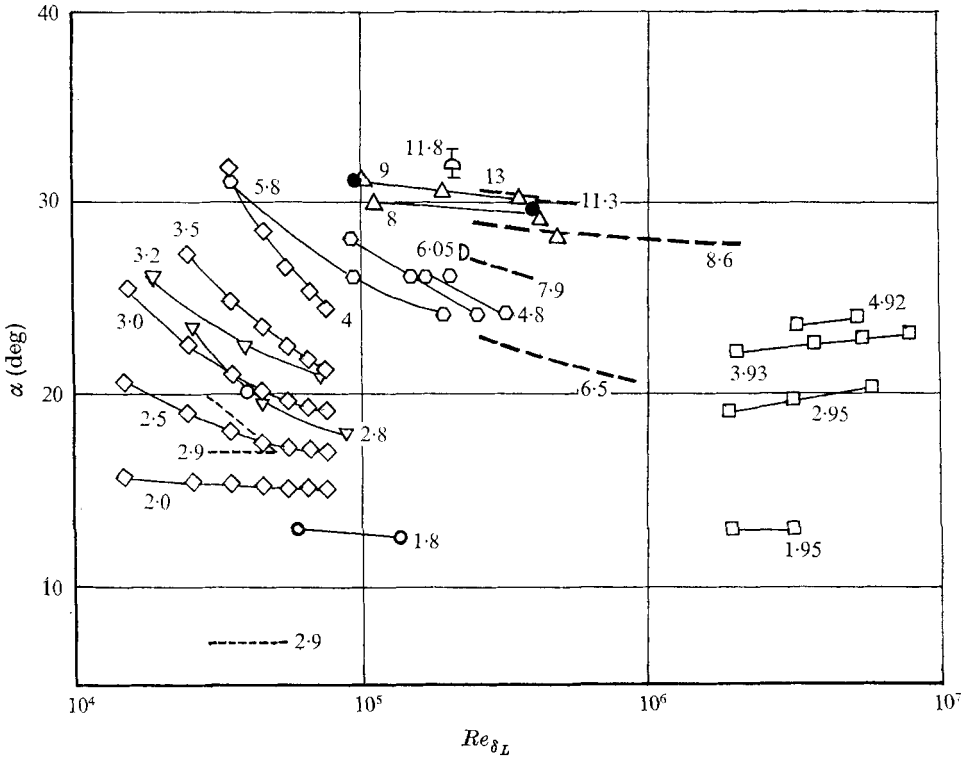

FIGURE 8. Incipient separation at a wedge compression corner. ⌓, Appels & Backx (1971), $T_w = 0{\cdot}13T_r$; ●, present study, $T_w = 0{\cdot}3T_r$; ○, Drougge (1953), $T_w = T_r$; △, Elfstrom (1972), $T_w = 0{\cdot}3 \to 0{\cdot}7\,T_r$; ▷, Gray & Rhudy (1971), $T_w = T_r$; ———, Holden (1972), $T_w = 0{\cdot}17 \to 0{\cdot}4T_r$; ▽, Kessler, Reilly & Mockapetris (1970), $T_w = T_r$; ◇, Kuehn (1959), $T_w = T_r$; □, Roshko & Thomke (1969), $T_w = T_r$; – – –, Spaid & Frishett (1972), $T_w < T_r$; ⬡, Sterrett & Emery (1962), $T_w = T_r$.

angle α_i slightly (figure 7). This trend agrees well with that found by Elfstrom (1972), Batham (1972) and many other investigators but, the opposite trend has been measured by Roshko & Thomke (1969), Green (1971) and Hammitt & Hight (1959) and may be associated with the slow variation of the turbulent boundary-layer profile with momentum-thickness Reynolds number. Immediately after transition the wake component of the profile is absent and at hypersonic speeds seems slow to develop. The corresponding profile is very 'full' and the boundary layer is difficult to separate. As the wake components develops so the profile wanes and the incipient separation angle falls with rising Reynolds number. However, once the wake component is fully developed a further increase in Reynolds number causes the profile to expand again since the wall and wake components grow at different rates. This is sometimes described by stating that n increases in the power-law profile $(u/u_\infty) = (y/\delta)^{1/n}$. Previous experiments by Coleman, Elfstrom & Stollery (1971) have shown that all of the present data fall in the range where the wake component is still developing. The incipient separation measurements confirm those of Elfstrom made under the same test conditions. They have been added to other currently available results in figure 8.

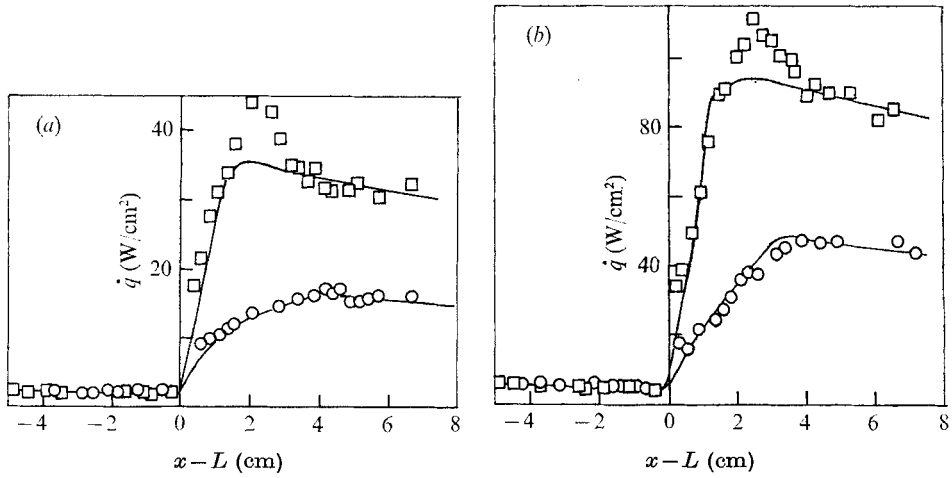

FIGURE 9. Comparison of experiment and theory for the present results. (*a*) $M_\infty = 8{\cdot}96$, $Re_\infty = 1{\cdot}2 \times 10^5\,\mathrm{cm}^{-1}$; $T_0 = 1070\,^\circ\mathrm{K}$, $T_w = 295\,^\circ\mathrm{K}$. (*b*) $M_\infty = 9{\cdot}22$, $Re_\infty = 4{\cdot}7 \times 10^5\,\mathrm{cm}^{-1}$; $T_0 = 1070\,^\circ\mathrm{K}$, $T_w = 295\,^\circ\mathrm{K}$. □, $\alpha = 30^\circ$; ○, $\alpha = 15^\circ$; ———, predictions.

In order to use the theory described in § 3 the pressure distribution is needed. Elfstrom has described a simple method of calculating the pressure and the calculation rather than his measurements have been used in order to test the heat-transfer theory as a prediction technique. Having calculated p_e and knowing the downstream reservoir conditions from the oblique shock relations the local edge conditions were obtained from the isentropic relations.

$$\left(\frac{p_e}{p_{02}}\right)^{(\gamma-1)/\gamma} = \left(\frac{\rho_e}{\rho_{02}}\right)^{\gamma-1} = \frac{T_e}{T_{02}} = \left(1+\frac{\gamma-1}{2}M_e^2\right)^{-1}.$$

This calculation procedure has been used to predict the heat transfer for attached flow at $\alpha = 15^\circ$ and 30° using a Reynolds analogy factor ($Pr^{-\frac{2}{3}}$) of 1·16. The predictions are compared with the measurements in figure 9 and the agreement is very encouraging.

Thomann (1967) used a similar theoretical method due to Crabtree, Dommett & Woodley (1965) to make estimates for comparison with his own experimental data taken at $M = 2{\cdot}5$ using a curved compression corner model. Figure 10(*a*) shows this comparison together with the prediction of equation (6). Figure 10(*b*) shows one further comparison between the simple theory presented here and the recent data of Holden (1972) at $M = 8.6$. Once again agreement is good.

5. Conclusions

Experiments have been made which extend the range of existing turbulent boundary layer shock-wave interaction data. The heat-transfer-rate distributions over compression corners closely follow the form of the pressure distribution, the rise of heat-transfer rate in the separated region being a notable feature. Using the method of Elfstrom to calculate the pressure distribution a simple theory

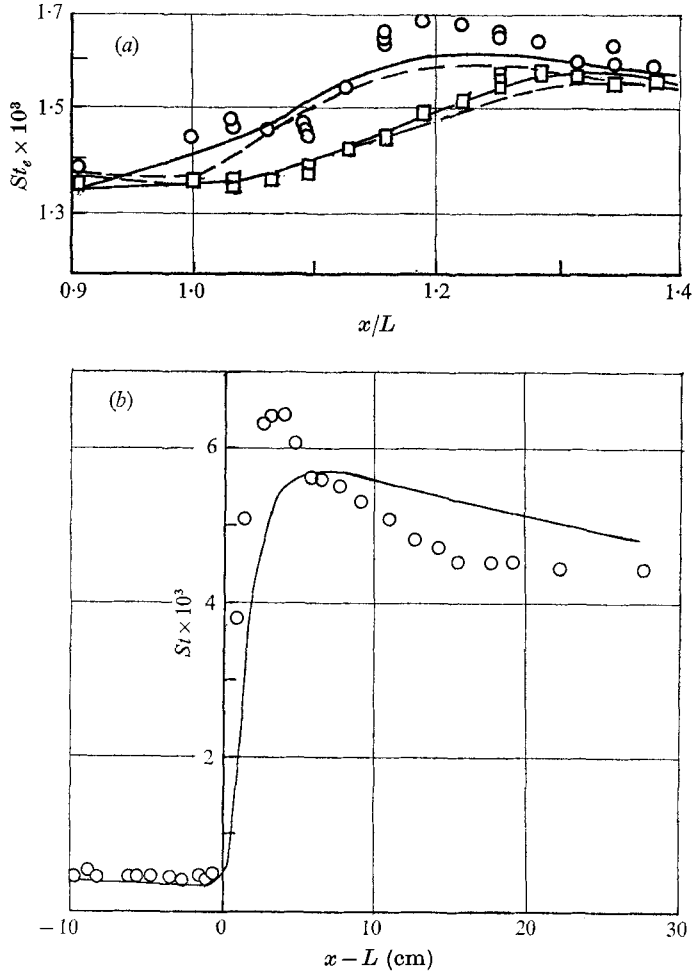

FIGURE 10. Comparison of theory with other sources of data. (*a*) Thomann (1967). Flat plate plus trailing edge flap: curved compression corner. $M_\infty = 2.5$, $T_0 = 290$ °K, $T_w = 212{\cdot}5$ °K, $Re_\infty = 1{\cdot}01 \times 10^5\,\mathrm{cm}^{-1}$, $L = 31{\cdot}75$ cm, $\alpha = 20°$, ○, corner radius = 15 cm; □, corner radius = 30 cm; ———, predictions of current method; '——, predictions of Crabtree *et al.* (1965). (*b*) Holden (1972). Wedge compression corner model. $M_\infty = 8{\cdot}6$, $T_0 = 1011$ °K, $T_w/T_0 = 0{\cdot}3$, $Re_\infty = 3{\cdot}22 \times 10^5\,\mathrm{cm}^{-1}$, $L = 68{\cdot}6$ cm, $\alpha = 27°$. ———, prediction of current method.

based on an overall heat balance plus local flat-plate similarity can give good estimates of the heat transfer for attached flow. The peak heat-transfer rate in the turbulent reattachment region can exceed laminar stagnation point values.

This research was sponsored by the Ministry of Defence under contract AT/2037/057.

REFERENCES

AMBROK, G. S. 1957 *Soviet Phys.* **2** 1979.

APPELS, C. & BACKX, E. 1971 *VKI Student Rep.*

BACK, L. H. & CUFFEL, R. F. 1970 *A.I.A.A. J.* **8**, 1871.

BATHAM, J. P. 1972 *J. Fluid Mech.* **52**, 425–435.

CERESUELA, R. & COULOMB, J. 1970 *L'Aeronautique et L'Astronautique*, **18**, 15–28.

CHAPMAN, D. R. 1956 *N.A.C.A. Tech. Note*, no. 3792.

COLEMAN, G. T., ELFSTROM, G. M. & STOLLERY, J. L. 1971 *AGARD Conf. Proc. on Turbulent Shear Flows*, no. 93.

COLEMAN, G. T. & STOLLERY, J. L. 1972 *Imperial College Aero Rep.* no. 72–05.

CRABTREE, L. F., DOMMETT, R. L. & WOODLEY, J. G. 1965 *R.A.E. Tech. Rep.* no. 65137.

DROUGGE, G. 1953 *F.F.A. Rep.* no. 47. Sweden.

ECKERT, E. R. G. 1956 *Trans. A.S.M.E.* **78**, 1273.

ELFSTROM, G. M. 1972 *J. Fluid Mech.* **53**, 113–127.

GADD, G. E. COPE, W. F. & ATTRIDGE, J. L. 1960 *Aero. Res. Counc. Tech. Rep.* no. 3148.

GRAY, J. D. & RHUDY, R. W. 1971 *AEDC-Tr*-70-235.

GREEN, J. E. 1971 *R.A.E. Rep.* To be published.

HAMMITT, A. G. & HIGHT, S. 1959 *AFOSR Tech. Note*, no. 60–82.

HOLDEN, M. S. 1972 *A.I.A.A. Paper*, no. 72–74.

HOLLOWAY, P. F., STERRETT, J. R. & CREEKMORE, H. S. 1965 *N.A.S.A. Tech. Note*, D-3074.

KUEHN, D. M. 1959 *NASA Memo.* no. 1-21-59A.

KESSLER, W. C., REILLY, J. F. & MOCKAPETRIS, L. V. 1970 *McDonnell Douglas Corp. Rep.* MOC 59800.

LEES, L. & REEVES, B. L. 1964 *A.I.A.A. J.* **2**, 1907–1920.

NEEDHAM, D. A., ELFSTROM, G. M. & STOLLERY, J. L. 1970 *Imperial College Aero Rep.* no 70–04.

ROSHKO, A. & THOMKE, G. J. 1969 *A.R.L. Symp. on Viscous Interaction Phenomena in Supersonic and Hypersonic Flow.* University of Dayton Press.

SPAID, F. W. & FRISHETT, J. C. 1972 *A.I.A.A. J.* **10**, 915–922.

STERRETT, J. R. & EMERY, J. C. 1962 *N.A.S.A. Tech. Note*, D-1014.

THOMANN, H. 1967 *F.F.A. Rep.* no. 113. Sweden.

TODISCO, A. & REEVES, B. L. 1969 *A.R.L. Symp. on Viscous Interaction Phenomena in Supersonic and Hypersonic Flow.* University of Dayton Press.

WALKER, G. K. 1960 *J. Aero Sci.* **27**, 715–716.

FIGURE 1. Schlieren pictures of the flow at a wedge compression corner. $M_\infty = 8{\cdot}96$, $Re_{\delta_1} = 0{\cdot}93 \times 10^5$. (*a*) $\alpha = 15$°. (*b*) $\alpha = 30$°. (*c*) $\alpha = 34$°. (*d*) $\alpha = 38$°.

(*Facing p. 752*)